

Structural Transition and the Electronic/Magnetic Properties of Oxidized Ca_2N Electrenes

Pedro H. Souza¹, José E. Padilha², and Roberto H. Miwa^{1*}

¹*Instituto de Física, Universidade Federal de Uberlândia,
C.P. 593, 38400-902, Uberlândia, MG, Brazil and*

²*Campus Avançado Jandaia do Sul,
Universidade Federal do Paraná,
86900-000, Jandaia do Sul, PR, Brazil.*

(Dated: June 4, 2022)

Based on first-principles calculations we show that the oxidation of ultrathin films of Ca_2N electrides, electrenes, drives a hexagonal \rightarrow tetragonal structural transition. The ground state configuration of the oxidized monolayer (ML) and bilayer (BL) systems can be viewed as CaO/CaN and $\text{CaO}/(\text{CaN})_2/\text{CaO}$ two dimensional (2D) heterostructures. In both systems, the nearly free electron (NFE) states lie near the vacuum level, where the spatial projection reveals that they are localized above the oxidized CaO surface. Focusing on electronic and magnetic properties, we find that the nitrogen atoms of the oxidized Ca_2N becomes spin-polarized ($\sim 1 \mu_B/\text{N-atom}$); where (i) the ferromagnetic and the anti-ferromagnetic phases are nearly degenerated in the ML system, CaO/CaN , while (ii) there is an energetic preference for the ferromagnetic phase in $\text{CaO}/(\text{CaN})_2/\text{CaO}$. We show that such a FM preference can be strengthened upon mechanical compression. The FM $\text{CaO}/(\text{CaN})_2/\text{CaO}$ presents a half-metallic electronic band structure, where the metallic channels project (predominantly) on the $\text{N-}2p_{x,y}$ orbitals. In addition to the total energy results, further molecular dynamic and phonon spectra calculations have been done in order to verify its thermal and structural stability. Those findings suggest that $\text{CaO}/(\text{CaN})_2/\text{CaO}$ is a quite interesting, and structurally stable, 2D FM heterostructure characterized half-metallic bands sandwiched by NFE states lying on the oxidized surfaces.

I. INTRODUCTION

Two dimensional (2D) materials have been the subject of numerous studies addressing technological applications as well as fundamental issues. The seminal work on graphene[1] boosted the synthesis of other 2D systems. For instance, transition metal dichalcogenides,[2, 3] obtained through exfoliation processes of their layered parents, and 2D boron sheets (borophene) synthesized by bottom-up techniques on metal surfaces.[4, 5] In parallel to the experimental realizations, computational simulations have played an important role performing a virtual engineering on 2D systems; proposing new materials, and providing an atomic understanding of their physical/chemical properties.[6–8] The combination of those efforts has contributed to the current revolution in the material science based on 2D structures.[9]

Further control on the physical properties of those 2D material can be done by tuning structural parameters like (i) the number of stacked layers or (ii) the equilibrium lattice structure; *e.g.* in (i) we have the linear/parabolic energy dispersion in graphene monolayer/bilayer,[10–13] while in (ii) the semiconducting/metallic electronic structure of 2H/1T MoS_2 . [14–17] More elaborate strategies have been proposed/applied in order to tailor the electronic properties of those 2D systems, as the design of van der Waals (vdW) heterostructures by stacking combinations of 2D materials[18–20], functionalization by foreign

elements,[21–23] and synthesis of Janus structures.[24–27]

It is worth noting that low dimensional systems, like bundles of carbon nanotubes and fullerenes host nearly free electron (NFE) states.[28–30] In fact, NFE states have been firstly detected on metal surfaces through inverse photoemission spectroscopy experiments,[31–33] and confirmed by first-principles calculations.[34–38] Such NFE states are also present in 2D systems. For instance, in graphene those states were measured by near edge x-ray spectroscopy, [39] and further supported by theoretical first-principles DFT calculations.[40]

Two dimensional dicalcium nitride is a layered system which hosts NFE states. Each Ca_2N layer unit is composed by a nitrogen atomic sheet sandwiched by calcium layers connected by Ca-N-Ca chemical bonds, whereas the Ca_2N units are stacked along the (001) direction bounded by van der Waals (vdW) interactions. Based on the oxidation states of Ca^{2+} and N^{3-} atoms, we can infer that each Ca_2N unit is positively charged, $[\text{Ca}_2\text{N}]^+$, and thus in order to provide electrostatic stability to the system, negative charges (anionic electron) take place between the Ca_2N layers.[41, 42] The NFE states are partially occupied by those anionic electrons, giving rise to metallic bands for wave-vectors on the [001] plane.[43] Meanwhile, in few layer systems, it has been predicted the presence of the anionic electrons not only embedded between the Ca_2N layers, but also on the surface region of the slab, giving rise to (metallic) NFE surface states.[44]

Few years ago, 2D nanosheet systems of Ca_2N electrides (electrenes) have been successfully synthesized

* hiroki@ufu.br

through exfoliation processes.[45] In fact, the metallic character, ruled by ionic electrons, was already predicted in the Ca_2N monolayer systems.[46] Since the presence of metallic surface states makes the Ca_2N electrenes chemically very reactive,[47] it has been proposed some strategies aiming to circumvent such a problem. For instance, the encapsulation of the Ca_2N nanosheet using 2D shields like graphene, single layer of BN, or graphane.[46] On the other hand, NFE states make the Ca_2N surface a quite interesting platform to perform atomic design on 2D materials,[48] for instance through functionalization by foreign atoms or molecules.[49–54] Indeed, OH-functionalized Ca_2N and Y_2C monolayers have been proposed as new 2D materials for application in ion batteries;[55] and very recently, it has been proposed the control of the electronic and magnetic properties in Ca_2N monolayers through hydrogenation and oxidation.[56, 57] processes.

Finally, it is well known that, in order to minimize the surface free energy, the surface atoms may rearrange upon incorporation of foreign elements. Such surface reconstructions may result in noteworthy electronic properties. For instance, the formation of NFE states and the nearly 1D metallic transport channels on the (single layer) indium covered silicon surface, $\text{In}/\text{Si}(111)-(\sqrt{7} \times \sqrt{3})$. [58, 59]

Once it is reasonable to infer that such an atomic rearrangements may take place in functionalized 2D systems; here, based on the density functional theory (DFT), we performed a set of first-principles calculations of the fully oxidized monolayer (ML) and bilayer (BL) Ca_2N electrenes. Our total energy results reveal a hexagonal \rightarrow tetragonal structural transition in the oxidized Ca_2N -ML and -BL, resulting in 2D tetragonal heterostructures composed by stacked layers of CaO and CaN , namely CaO/CaN and $\text{CaO}/(\text{CaN})_2/\text{CaO}$, respectively. In the sequence, the perform a detailed study of the electronic and magnetic properties of those systems. We found that both oxidized electrenes are metallic; where the ferromagnetic phase is strengthened in the bilayer system. $\text{CaO}/(\text{CaN})_2/\text{CaO}$ is characterized by half-metallic bands localized within the $(\text{CaN})_2$ layers, sandwiched by NFE states lying on the oxidized CaO surface. Molecular dynamics and phonon spectra calculation were done in order to confirm the thermal and structural stability of $\text{CaO}/(\text{CaN})_2/\text{CaO}$. Those findings suggest that $\text{CaO}/(\text{CaN})_2/\text{CaO}$ is a potential structure for application in 2D nanodevices.

II. COMPUTATIONAL DETAILS

The calculations were performed by using the density functional theory (DFT),[60] as implemented in the computational codes Quantum-Espresso (QE)[61] and Vienna Ab initio Simulation Package (VASP).[62, 63] We have considered the generalized gradient approximation of Perdew-Burke-Ernzerhof (GGA-PBE) [64] for the

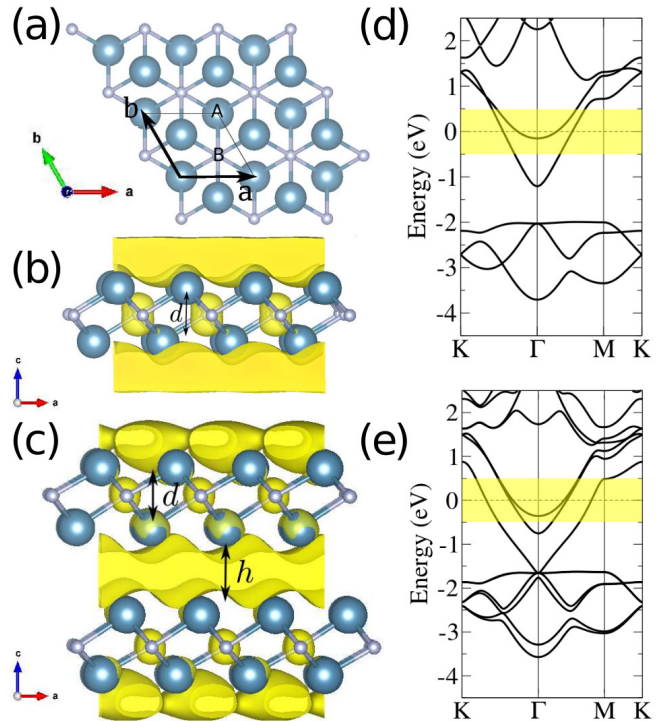


FIG. 1. Structural model of Ca_2N -1ML, top-view (a), side-view and the partial electron charge density within an energy interval of $E_F \pm 0.5$ eV of Ca_2N -ML (b) and can-BL (c). Electronic band structure of Ca_2N -ML (d) and -BL (e). Isosurfaces of 0.002 (b) and 0.005 $e/\text{\AA}^3$.

exchange-correlation functional. The Kohn-Sham [65] orbitals, and the self-consistent total charge density were expanded in plane wave basis sets with energy cutoffs of 70 and 353 Ry, respectively. The Brillouin zone sampling was performed by using a $8 \times 8 \times 1$ k-point mesh.[66] The Ca_2N -ML and -BL systems were described within the supercell approach with surface periodicities of (1×1) , $(\sqrt{2} \times \sqrt{2})$, and (3×3) , and a vacuum region of between 22 and 28 \AA . The atomic positions were relaxed until the residual forces were converged to within 5 meV/ \AA , and the structural relaxation (variable-cell) was performed within a pressure convergence of 0.05 Kbar. The long-range van der Waals (vdW) interactions were described using the semiempirical approaches vdW-D2 and -D3.[67, 68] We have also checked the validity of our results using the self-consistent vdW-DF approach.[69–71]

The structural stability was verified through the calculation of elastic constants and the phonon dispersion using PHONOPY code;[72] and the thermal stability was verified by *ab initio* molecular dynamics simulations (AIMD) at 300 K, with a time step of 1 fs using Nosé heat bath scheme.[73]

III. RESULTS AND DISCUSSIONS

Pristine ML and BL Ca_2N . In Fig. 1 we present

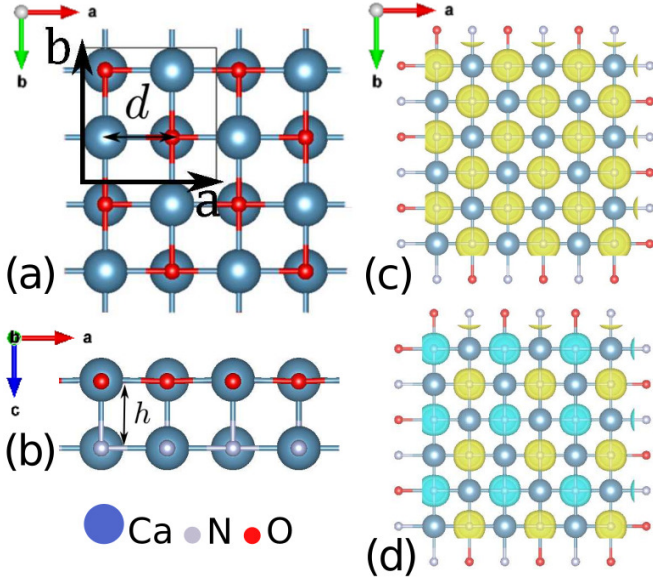


FIG. 2. Structural model of the fully oxidized $\text{Ca}_2\text{N-ML}$, forming tetragonal CaO and CaN stacked layers, CaO/CaN , top-view (a), and side-view (b). Spin-densities of the (c) FM and (d) AFM CaO/CaN . The spin-densities are localized on the nitrogen atoms. Isosurfaces of $0.005 e/\text{\AA}^3$.

the structural models and the electronic structure of pristine $\text{Ca}_2\text{N-ML}$ and -BL . In Ca_2N the N atoms are intercalated by Ca atoms, forming a triangular lattice, Fig. 1(a). At the equilibrium geometry, the $\text{Ca}_2\text{N-ML}$ presents a lattice constant (a) of 3.56 \AA , and Ca-Ca vertical distance (d) of 2.51 \AA [Fig. 1(b)]. The $\text{Ca}_2\text{N-BL}$ presents practically the same values of a and d , and interlayer distance $h = 3.62 \text{ \AA}$, Fig. 1(c). The energetic stability of the bilayer system is dictated by vdW interactions, where we found an interlayer binding energy of 79 meV/\AA^2 (1.26 J/m^2). The electronic band structures of $\text{Ca}_2\text{N-ML}$ and -BL , Figs. 1(d) and (e), reveal the formation of parabolic metallic bands for wave vectors parallel to the Ca_2N surface layer. The real space projection of those metallic parabolic bands within an energy interval of $\pm 0.5 \text{ eV}$ with respect to the Fermi level, $E_F \pm 0.5 \text{ eV}$, reveals the formation nearly free electron (NFE) states spreading out on the surface of $\text{Ca}_2\text{N-ML}$ and -BL , and sandwiched between Ca_2N layers in the BL system, Figs. 1(b) and (c).

Oxygen adsorption. Once we have characterized the electronic and structural properties of pristine $\text{Ca}_2\text{N-ML}$ and -BL , where we found a good agreement with the current literature,[41–43, 45, 46, 74, 75] in the sequence we examine their functionalization by oxygen adatoms.

The energetic stability of the oxidized systems was inferred through the calculation of the oxygen adsorption energy (E^a),

$$E^a = E[\text{Ca}_2\text{N}] + E[\text{O}_2]/2 - E[\text{O/Ca}_2\text{N}],$$

where $E[\text{O/Ca}_2\text{N}]$ and $E[\text{Ca}_2\text{N}]$ are the total energies of oxidized and pristine Ca_2N (ML or BL), and $E[\text{O}_2]$

is the total energy of an isolated O_2 molecule. Positive values of E^a indicate exothermic processes. In addition, in order to verify the emergence of magnetic phases, we compare the total energies of non-magnetic (E^{NM}) and magnetic (E^{Mag}) $\text{O/Ca}_2\text{N}$, $\Delta E^{\text{mag}} = E^{\text{NM}} - E^{\text{Mag}}$.

Firstly we calculate the adsorption energies of a single O adatom on the $\text{Ca}_2\text{N-ML}$. We have considered the sites A and B [Fig. 1(a)] in a (3×3) surface, and we found an energetic preference of 0.30 eV for the oxygen adatom lying on the hollow site (A), which is aligned with the Ca atom at the opposite side of the $\text{Ca}_2\text{N-ML}$. We obtained E^a of 4.94 eV/O-atom , thus confirming the dissociative adsorption of O_2 molecules on the Ca_2N surface.[46, 76]

For a full coverage of oxygen adatoms, we found a structural transition of the oxidized $\text{Ca}_2\text{N-ML}$, $\text{O/Ca}_2\text{N-ML}$. We have considered the hexagonal lattice of pristine $\text{Ca}_2\text{N-ML}$ as the initial configuration, and upon structural and atomic relaxations, we found (i) a metastable phase where the lattice vectors \mathbf{a} and \mathbf{b} increase by 12.5% with respect to the pristine $\text{Ca}_2\text{N-ML}$, and the planar angle between \mathbf{a} and \mathbf{b} (γ) increases from 120° to 125° , followed by (ii) a ground state tetragonal lattice with $|\mathbf{a}| = |\mathbf{b}| = 4.72 \text{ \AA}$ [Fig. 2(a)], and more stable than (i) by $0.97 \text{ eV/(1} \times \text{1)}$ ($E^a = 4.04 \text{ eV/O-atom}$). Pointing out a large thermodynamic preference for (ii). As shown in Fig. 2(b), $\text{O/Ca}_2\text{N-ML}$ is characterized by parallel layers of CaO and CaN , each one forming planar square-lattices with Ca-O and Ca-N bond lengths of 2.36 \AA [d in Fig. 2(a)] connected by Ca-O vertical bonds [$h = 2.45 \text{ \AA}$ in Fig. 2(b)]. Such a tetragonal phase of $\text{O/Ca}_2\text{N-ML}$ can be described as a layered combination of trigonal structures of CaO and CaN crystals,[77] forming a 2D CaO/CaN heterostructure. We can infer that the structural preference for the tetragonal phase is attributed to the larger formation energy of CaO [78] compared with that of Ca_2N . [79]

Focusing on the magnetic properties, there is an energy gain of $\Delta E^{\text{mag}} = 68 \text{ meV/(1} \times \text{1)}$ upon the inclusion of spin-polarization. We found a net magnetization (m) of $1 \mu_B$ localized on the N atoms, a shown in Figs. 2(c) and (d) for the FM and AFM phases, respectively. The total energy comparison between the FM (E^{FM}) and AFM (E^{AFM}) phases indicates that the former is slightly more stable, with $E^{\text{AFM}} - E^{\text{FM}} = 7.6 \text{ meV/N-atom}$. Here, the emergence of such a magnetic phase in CaO/CaN can be considered as a remnant property of the (trigonal) CaN crystal. Electronic band structure calculations indicate the formation of metallic bands for both spin configurations (FM and AFM). The energy bands of the FM CaO/CaN [Fig. 3(a)], and the projection of the electronic states near the Fermi level [$-0.15 < E - E_F < 0.5 \text{ eV}$ in Fig. 3(c)] reveals a half-metallic system ruled by the $\text{N-}2p_{x,y}$ orbitals. It is worth noting that such a half-metallic behavior is suppressed in the AFM CaO/CaN . Further projection of the energy bands onto the atomic orbitals of Ca, N, and O [Fig. 3(b)] indicates that there are no atomic orbital contributions to the lowest unoccupied parabolic band $c1$. Indeed, its spatial distribu-

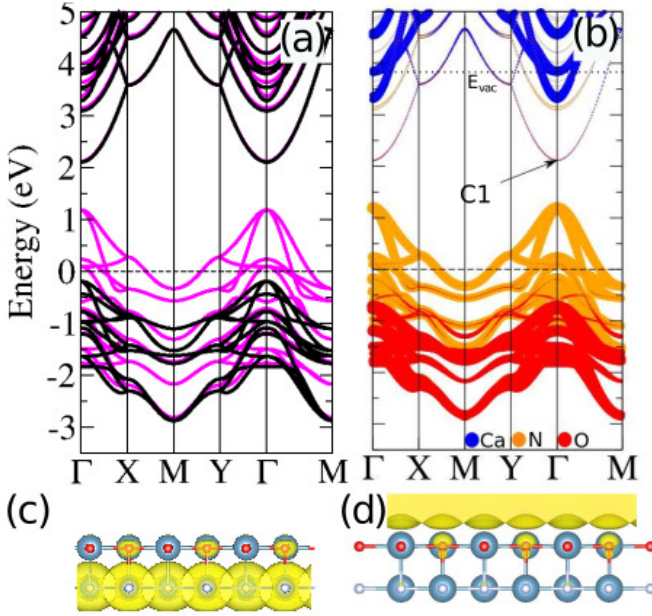


FIG. 3. (a) Spin-polarized electronic band structure of the FM-CaO/CaN, (b) projection of the energy bands onto atomic orbitals; spacial projection of the metallic bands near the Fermi level ($E_F \pm 0.2$ eV) (c), and the parabolic band (c1) near the Γ -point (d). Isosurfaces of $0.001 e/\text{\AA}^3$.

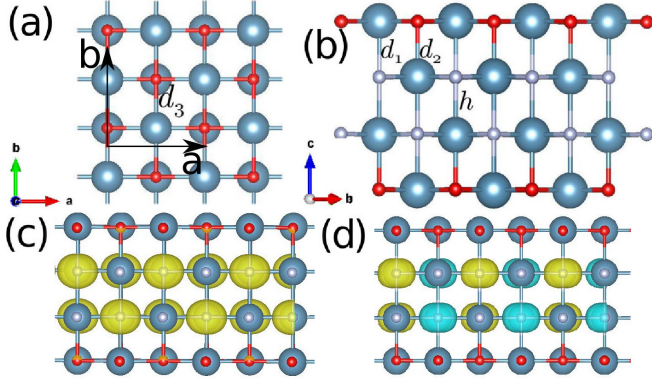


FIG. 4. Structural model of $\text{CaO}/(\text{CaN})_2/\text{CaO}$, (a) top-view, and (b) side-view. The bond lengths d_i ($i=1, 2$, and 3) are 2.47, 2.40, and 2.39 \AA , respectively, and $h = 2.53$ \AA . Spin-densities of the (c) FM and (d) AFM phases. Isosurfaces = $0.005 e/\text{\AA}^3$.

tion near the Γ point, spreading out on the CaO surface [Fig. 3(d)], allow us to identify c1 as a NFE band localized at ~ 1.6 eV below the vacuum level (E_{vac}).

We next have considered the oxidation of both sides of $\text{Ca}_2\text{N-BL}$, $\text{O}/\text{Ca}_2\text{N-BL}/\text{O}$. Similarly to what we have done in $\text{O}/\text{Ca}_2\text{N-ML}$, we took the hexagonal structure of pristine $\text{Ca}_2\text{N-BL}$ as the starting configuration. By performing full structural and atomic relaxations, we found a tetragonal lattice more stable than the hexagonal one by $1.97 \text{ eV}/(1 \times 1)$. At the ground state configuration, we

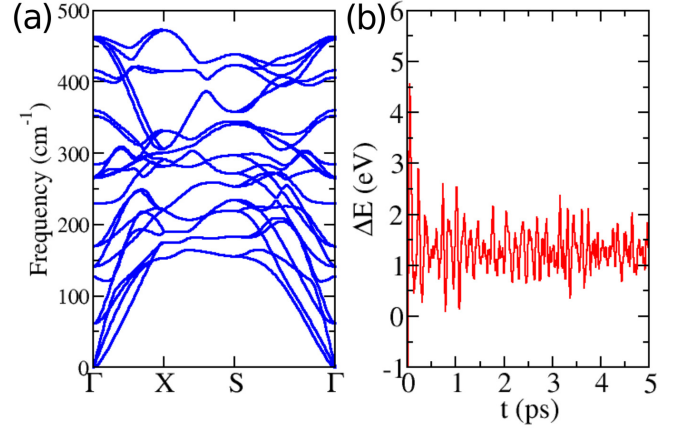


FIG. 5. (a) Phonon dispersion for $\text{O}/\text{Ca}_2\text{N-BL}/\text{O}$. (b) Energy Fluctuation at 300K. The insets, show snapshots of the crystal structures for a time of 5ps.

found $|a|=|b|=4.77 \text{ \AA}$ as shown in Fig. 4(a), where the oxidation process is exothermic by $E^a = 4.14 \text{ eV/O-atom}$. That is, the dissociative adsorption picture has been kept for O_2 molecule on the $\text{Ca}_2\text{N-BL}$ surface. $\text{O}/\text{Ca}_2\text{N-BL}/\text{O}$ can be viewed as a combination of two CaO/CaN structures. However, instead of vdW interaction, the formation of C-N chemical bonds, indicated as h in Fig. 4(b), increases the interlayer binding energy from 79 meV/\AA^2 (pristine $\text{Ca}_2\text{N-BL}$) to 93 meV/\AA^2 . The equilibrium geometry of $\text{O}/\text{Ca}_2\text{N-BL}/\text{O}$ is characterized by an inner region that mimics the atomic structure of the trigonal CaN, sandwiched by nearly planar layers of CaO, $\text{CaO}/(\text{CaN})_2/\text{CaO}$.

In addition to the energetic stability of $\text{CaO}/(\text{CaN})_2/\text{CaO}$, discussed above, we have also examined its (i) structural, and (ii) thermal stabilities. The former [(i)], was performed by the calculation the phonon spectra, presented in Fig. 5(a). We have considered the finite-displacement approach, with supercell sizes of (3×3) primitive unit cells. As we can see, the phonon frequencies are all real (no imaginary frequencies). Those results allow us to infer that those systems are structurally stable. In (ii), we have performed *ab initio* molecular dynamics (AIMD) simulations at 300K, with a time step of 1 fs using the Nosé heating bath scheme.[73] We have constructed a (3×3) supercell containing 9 formula units to minimize the constraint induced by the slab periodicity. The results of the variations of the total potential energy with respect to the simulation time, and snapshots of the last configurations are presented in Fig. 5(b). As we can observe, the atomic configuration remains nearly unaltered up to 5 ps, and no phase transition is observed in the total potential energy. These results demonstrate that the 2D $\text{CaO}/(\text{CaN})_2/\text{CaO}$ material, once synthesized, is stable and preserving its structural integrity at room temperature.

We next explored the magnetic and electronic proper-

ties of $\text{CaO}/(\text{CaN})_2/\text{CaO}$. There is an energy gain upon the inclusion of spin-polarization of $\Delta E^{\text{mag}}=70$ meV/N-atom, practically the same as that obtained in CaO/CaN . The net magnetization is mostly localized on the N atoms, with $\sim 1\mu_B/\text{N-atom}$. Further comparison between the FM and AFM couplings revealed that, (i) there is an energetic preference of 21 meV/N-atom for the FM configuration between the nitrogen atoms lying on the same CaN layer (intralayer coupling), and (ii) between the stacked CaN layers (interlayer coupling) we found the FM phase [Fig. 4(c)] more stable than the AFM phase [Fig. 4(d)] by 32 meV/N-atom. Here, the formation of the FM phase in $\text{CaO}/(\text{CaN})_2/\text{CaO}$ can be considered as a remnant property of CaN trigonal crystal. Using the mean field theory, we estimate a Curie temperature (T_C) in (i) of 162 K.[80]

It is worth noting that although nearly the same energy gain due to the spin-polarization (ΔE^{mag}), the energetic preference for the intralayer FM configuration has been strengthened in $\text{CaO}/(\text{CaN})_2/\text{CaO}$; *i.e.* $E^{\text{AFM}} - E^{\text{FM}} = 7.6 \rightarrow 21$ meV/N-atom. Such a preference can be attributed to the FM interlayer coupling [(ii)]. In this case, we can infer that such an energetic preference of the FM phase can be tuned by a compressive strain normal to the 2D $\text{CaO}/(\text{CaN})_2/\text{CaO}$, and thus, increasing the Curie temperature. Indeed, this is what we found by compressing the $\text{CaO}/(\text{CaN})_2/\text{CaO}$ by 3 % normal to the stacking direction. The strength of the FM phase ruled by the interlayer coupling increased from 32 to 60 meV/N-atom.

The electronic band structure of the FM $\text{CaO}/(\text{CaN})_2/\text{CaO}$ characterizes a half-metal system, Fig. 6(a), where the metallic channels are (mostly) ruled by the N- $2p_{x,y}$ orbitals. Figure 6(c) shows the charge density distribution of the metallic bands within $E_F \pm 0.2$ eV. Further energy band projections [Fig. 6(b)] reveal that the unoccupied parabolic bands c1 and c2, lying at ~ 1.1 eV (Γ -point) below the vacuum level, present no contributions from the atomic orbitals. Instead, c1 and c2 project on plane-waves characterizing NFE states spreading out (symmetrically) on the oxidized CaO surfaces as shown in Fig. 6(d). That is, the fully oxidized Ca_2N -BL, $\text{CaO}/(\text{CaN})_2/\text{CaO}$, presents a combination of half-metal channels along the $(\text{CaN})_2$ layers, sandwiched by NFE states on top of the oxidized CaO surface.

IV. SUMMARY AND CONCLUSIONS

We have performed a theoretical study, based on first-principles DFT calculations, of the oxidized Ca_2N electrenes. The structural and atomic relaxations of the fully oxidized Ca_2N -ML and -BL systems reveal a hexagonal

nal \rightarrow tetragonal structural transition, giving rise to CaO and CaN (covalently bounded) stacked layers. Those oxidized systems can be viewed as two-dimensional CaO/CaN and $\text{CaO}/(\text{CaN})_2/\text{CaO}$ heterostructures. Both systems are metallic, characterized by NFE states near the vac-

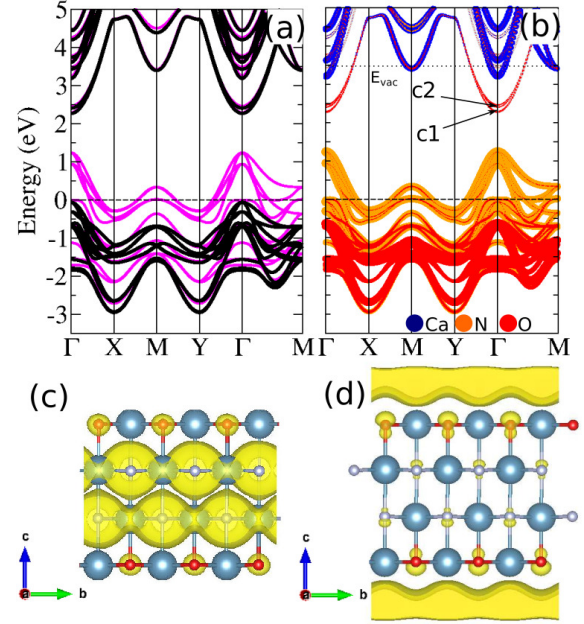


FIG. 6. Spin-polarized electronic band structure of the FM $\text{CaO}/(\text{CaN})_2/\text{CaO}$ (a), and spatial projection of the energy bands near the Fermi level ($E_F \pm 0.2$ eV) (c). (b) Projection of the energy bands on the Ca, N, and O atomic orbitals and spatial (d) the projection of the parabolic band c1. Isosurfaces of $0.001e/\text{\AA}^3$.

uum level, and localized above the oxidized CaO surfaces. The latter exhibits a (tuneable) FM phase (strength), where the magnetic moment is mainly localized on the nitrogen atoms; giving rise to half-metallic energy bands projected mostly on the N- $2p_{x,y}$ orbitals. The structural and thermal stabilities of $\text{CaC}/(\text{CaN})_2/\text{CaO}$ have been confirmed through phonon spectra and molecular dynamic calculations. Those findings suggest that $\text{CaC}/(\text{CaN})_2/\text{CaO}$, a half-metal intercalated by NFE states, is a promising 2D material to the development of nanodevices.

ACKNOWLEDGMENTS

The authors acknowledge financial support from the Brazilian agencies CNPq, CAPES, and FAPEMIG, and the CENAPAD-SP and Laboratório Nacional de Computação Científica (LNCC-SCAFMat2) for computer time.

[1] K. S. Novoselov, A. K. Geim, S. V. Morozov, D. Jiang, Y. Zhang, S. V. Dubonos, V. Grigoreva, and A. A.

Firsov, Science **306**, 666 (2004).

- [2] K. S. Novoselov, D. Jiang, F. Shedin, T. J. Booth, V. V. Khotkevich, S. V. Morozov, and A. K. Geim, *Proc. Natl. Acad. Sci. USA* **102**, 10451 (2005).
- [3] M. Chhowalla, H. S. Shin, G. Eda, L.-J. Li, K. P. Loh, and H. Zhang, *Nature Chemistry* **5**, 263 (2013).
- [4] A. J. Mannix, X.-F. Zhou, B. Kiraly, J. D. Wood, D. Alducin, B. D. Myers, X. Liu, B. L. Fisher, U. Santiago, J. R. Guest, *et al.*, *Science* **350**, 1513 (2015).
- [5] B. Feng, J. Zhang, Q. Zhong, W. Li, S. Li, H. Li, P. Cheng, S. Meng, L. Chen, and K. Wu, *Nature Chemistry* **8**, 563 (2016).
- [6] N. Mounet, M. Gibertini, P. Schwaller, D. Campi, A. Merkys, A. Marrazzo, T. Sohier, I. E. Castelli, A. Cepellotti, G. Pizzi, *et al.*, *Nature Nanotechnology* **13**, 246 (2018).
- [7] S. Hastrup, M. Strange, M. Pandey, T. Deilmann, P. S. Schmidt, N. F. Hinsche, M. N. Gjerding, D. Torelli, P. M. Larsen, A. C. Riis-Jensen, *et al.*, *2D Materials* **5**, 042002 (2018).
- [8] G. R. Schleder, A. C. Padilha, C. M. Acosta, M. Costa, and A. Fazzio, *Journal of Physics: Materials* **2**, 032001 (2019).
- [9] G. R. Bhimanapati, Z. Lin, V. Meunier, Y. Jung, J. Cha, S. Das, D. Xiao, Y. Son, M. S. Strano, V. R. Cooper, *et al.*, *ACS nano* **9**, 11509 (2015).
- [10] T. Ohta, A. Bostwick, T. Seyller, K. Horn, and E. Rotenberg, *Science* **313**, 951 (2006).
- [11] E. V. Castro, K. Novoselov, S. Morozov, N. Peres, J. L. Dos Santos, J. Nilsson, F. Guinea, A. Geim, and A. C. Neto, *Physical review letters* **99**, 216802 (2007).
- [12] Y. Zhang, T.-T. Tang, C. Girit, Z. Hao, M. C. Martin, A. Zettl, M. F. Crommie, Y. R. Shen, and F. Wang, *Nature* **459**, 820 (2009).
- [13] A. C. Neto, F. Guinea, N. M. Peres, K. S. Novoselov, and A. K. Geim, *Reviews of modern physics* **81**, 109 (2009).
- [14] Y.-C. Lin, D. O. Dumcenco, Y.-S. Huang, and K. Suenaga, *Nature nanotechnology* **9**, 391 (2014).
- [15] D. Voiry, A. Mohite, and M. Chhowalla, *Chemical Society Reviews* **44**, 2702 (2015).
- [16] G. Gao, Y. Jiao, F. Ma, Y. Jiao, E. Wacławik, and A. Du, *The Journal of Physical Chemistry C* **119**, 13124 (2015).
- [17] Y. Guo, D. Sun, B. Ouyang, A. Raja, J. Song, T. F. Heinz, and L. E. Brus, *Nano Letters* **15**, 5081 (2015).
- [18] A. K. Geim and K. S. Novoselov, *Nat. Mater.* **6**, 183 (2007).
- [19] K. Novoselov, A. Mishchenko, A. Carvalho, and A. C. Neto, *Science* **353**, aac9439 (2016).
- [20] C. Jin, E. Y. Ma, O. Karni, E. C. Regan, F. Wang, and T. F. Heinz, *Nature nanotechnology* **13**, 994 (2018).
- [21] D. Boukhvalov and M. Katsnelson, *Journal of Physics: Condensed Matter* **21**, 344205 (2009).
- [22] D. Chen, H. Feng, and J. Li, *Chemical reviews* **112**, 6027 (2012).
- [23] L. Yan, Y. B. Zheng, F. Zhao, S. Li, X. Gao, B. Xu, P. S. Weiss, and Y. Zhao, *Chemical Society Reviews* **41**, 97 (2012).
- [24] A.-Y. Lu, H. Zhu, J. Xiao, C.-P. Chuu, Y. Han, M.-H. Chiu, C.-C. Cheng, C.-W. Yang, K.-H. Wei, Y. Yang, *et al.*, *Nature nanotechnology* **12**, 744 (2017).
- [25] D. L. Duong, S. J. Yun, and Y. H. Lee, *ACS nano* **11**, 11803 (2017).
- [26] L. Dong, J. Lou, and V. B. Shenoy, *ACS nano* **11**, 8242 (2017).
- [27] F. Li, W. Wei, P. Zhao, B. Huang, and Y. Dai, *The Journal of Physical Chemistry Letters* **8**, 5959 (2017).
- [28] S. Okada, A. Oshiyama, and S. Saito, *Physical Review B* **62**, 7634 (2000).
- [29] J. Zhao, M. Feng, J. Yang, and H. Petek, *ACS nano* **3**, 853 (2009).
- [30] S. Hu, J. Zhao, Y. Jin, J. Yang, H. Petek, and J. Hou, *Nano letters* **10**, 4830 (2010).
- [31] P. Johnson and N. Smith, *Physical Review B* **27**, 2527 (1983).
- [32] B. Reihl, K. Frank, and R. Schlittler, *Physical Review B* **30**, 7328 (1984).
- [33] S. Hulbert, P. Johnson, N. Stoffel, W. Royer, and N. Smith, *Physical Review B* **31**, 6815 (1985).
- [34] A. Kiejna, *Physical Review B* **43**, 14695 (1991).
- [35] A. G. Eguiluz, M. Heinrichsmeier, A. Fleszar, and W. Hanke, *Physical review letters* **68**, 1359 (1992).
- [36] V. Silkin, E. Chulkov, and P. Echenique, *Physical Review B* **60**, 7820 (1999).
- [37] I. G. Hill and A. B. McLean, *Phys. Rev. Lett.* **82**, 2155 (1999).
- [38] R. H. Miwa and G. P. Srivastava, *Surf. Sci.* **473**, 123 (2001).
- [39] D. Pacilé, M. Papagno, A. F. Rodríguez, M. Grioni, L. Papagno, Ç. Girit, J. Meyer, G. Begtrup, and A. Zettl, *Physical review letters* **101**, 066806 (2008).
- [40] V. Silkin, J. Zhao, F. Guinea, E. Chulkov, P. Echenique, and H. Petek, *Physical Review B* **80**, 121408 (2009).
- [41] K. Lee, S. W. Kim, Y. Toda, S. Matsuishi, and H. Hosono, *Nature* **494**, 336 (2013).
- [42] A. Walsh and D. O. Scanlon, *Journal of Materials Chemistry C* **1**, 3525 (2013).
- [43] J. S. Oh, C.-J. Kang, Y. J. Kim, S. Sinn, M. Han, Y. J. Chang, B.-G. Park, S. W. Kim, B. I. Min, H.-D. Kim, *et al.*, *Journal of the American Chemical Society* **138**, 2496 (2016).
- [44] T. Inoshita, S. Takemoto, T. Tada, and H. Hosono, *Physical Review B* **95**, 165430 (2017).
- [45] D. L. Druffel, K. L. Kuntz, A. H. Woomer, F. M. Alcorn, J. Hu, C. L. Donley, and S. C. Warren, *Journal of the American Chemical Society* **138**, 16089 (2016).
- [46] S. Zhao, Z. Li, and J. Yang, *Journal of the American Chemical Society* **136**, 13313 (2014).
- [47] D. L. Druffel, A. H. Woomer, K. L. Kuntz, J. T. Pawlik, and S. C. Warren, *Journal of Materials Chemistry C* **5**, 11196 (2017).
- [48] R. J. Celotta, S. B. Balakirsky, A. P. Fein, F. M. Hess, G. M. Rutter, and J. A. Strosio, *Review of Scientific Instruments* **85**, 121301 (2014).
- [49] C. Weeks, J. Hu, J. Alicea, M. Franz, and R. Wu, *Phys. Rev. X* **1**, 021001 (2011).
- [50] K. K. Gomes, W. Mar, W. Ko, F. Guinea, and M. Har C, *Nature* **483**, 306 (2012).
- [51] C. Mera Acosta, Matheus P. Lima, R. H. Miwa, Antônio J. R. da Silva, and A. Fazzio, *Phys. Rev. B* **89**, 155438 (2014).
- [52] R. Drost, T. Ojanen, A. Harju, and P. Liljeroth, *Nature Physics* **13**, 668 (2017).
- [53] M. R. Slot, S. N. Kempkes, E. J. Knol, W. M. J. van Weerdenburg, J. J. van den Broeke, D. Wegner, D. Vanmaekelbergh, A. A. Khajetoorians, C. Morais Smith, and I. Swart, *Phys. Rev. X* **9**, 011009 (2019).
- [54] F. Crasto de Lima and R. Miwa, *Nano Letters* DOI: 10.1021/acs.nanolett.0c01111 (2020),

- <https://pubs.acs.org/doi/10.1021/acs.nanolett.0c01111>.
- [55] D. Wang, H. Li, L. Zhang, Z. Sun, D. Han, L. Niu, X. Zhong, X. Qu, and L. Yang, *Applied Surface Science* **478**, 459 (2019).
 - [56] X.-L. Qiu, J.-F. Zhang, Z.-Y. Lu, and K. Liu, *The Journal of Physical Chemistry C* **123**, 24698 (2019).
 - [57] C.-W. Wu and D.-X. Yao, *Journal of Magnetism and Magnetic Materials* **493**, 165727 (2020).
 - [58] E. Rotenberg, H. Koh, K. Rossnagel, H. Yeom, J. Schäfer, B. Krenzer, M. Rocha, and S. Kevan, *Physical review letters* **91**, 246404 (2003).
 - [59] S. Yamazaki, Y. Hosomura, I. Matsuda, R. Hobara, T. Eguchi, Y. Hasegawa, and S. Hasegawa, *Physical review letters* **106**, 116802 (2011).
 - [60] P. Hohenberg and W. Kohn, *Phys. Rev.* **136**, B864 (1964).
 - [61] P. Giannozzi *et al.*, *J. Phys.: Condens. Matter* **21**, 395502 (2009).
 - [62] G. Kresse and J. Furthmüller, *Comput. Mater. Sci.* **6**, 15 (1996).
 - [63] G. Kresse and J. Furthmüller, *Phys. Rev. B* **54**, 11169 (1996).
 - [64] J. P. Perdew, K. Burke, and M. Ernzerhof, *Phys. Rev. Lett.* **77**, 3865 (1996).
 - [65] W. Kohn and L. J. Sham, *Phys. Rev.* **140**, A1133 (1965).
 - [66] H. J. Monkhorst and J. D. Pack, *Phys. Rev. B* **13**, 5188 (1976).
 - [67] S. Grimme, *Journal of computational chemistry* **27**, 1787 (2006).
 - [68] S. Grimme, J. Antony, S. Ehrlich, and H. Krieg, *The Journal of chemical physics* **132**, 154104 (2010).
 - [69] M. Dion, H. Rydberg, E. Schröder, D. C. Langreth, , and B. I. Lundqvist, *Phys. Rev. Lett.* **92**, 246401 (2004).
 - [70] G. Roman-Perez and J. M. Soler, *Phys. Rev. Lett.* **103**, 096102 (2009).
 - [71] J. Klimeš, D. R. Bowler, and A. Michaelides, *Physical Review B* **83**, 195131 (2011).
 - [72] A. Togo and I. Tanaka, *Scripta Materialia* **108**, 1 (2015).
 - [73] S. Nosé, *The Journal of chemical physics* **81**, 511 (1984).
 - [74] C. Fang, G. de Wijs, R. de Groot, H. Hintzen, and G. de With, *Chemistry of materials* **12**, 1847 (2000).
 - [75] S. Liu, W. Li, S. W. Kim, and J.-H. Choi, *The Journal of Physical Chemistry C* **124**, 1398 (2020).
 - [76] L. Liu and H. L. Zhuang, *Mater. Res. Express* **5**, 076306 (2018).
 - [77] A. Jain, S. P. Ong, G. Hautier, W. Chen, W. D. Richards, S. Dacek, S. Cholia, D. Gunter, D. Skinner, G. Ceder, and K. a. Persson, *APL Materials* **1**, 011002 (2013).
 - [78] K. Persson, “Materials data on cao (sg:225) by materials project,” (2014).
 - [79] K. Persson, “Materials data on ca2n (sg:166) by materials project,” (2014), an optional note.
 - [80] J. Kudrnovský, I. Turek, V. Drchal, F. Máca, P. Weinberger, and P. Bruno, *Physical review B* **69**, 115208 (2004).